

Evolution of anomalous Hall effect in ferromagnetic Weyl semimetal $Nb_xZr_{1-x}Co_2Sn$

Bo-wen Chen(陈博文) and Bing Shen(沈冰)

Citation: Chin. Phys. B, 2024, 33 (**8**): 087501. DOI: 10.1088/1674-1056/ad4a3b

What follows is a list of articles you may be interested in

Tailoring-compensated ferrimagnetic state and anomalous Hall effect in quaternary Mn-Ru-V-Ga Heusler compounds

Jin-Jing Liang(梁瑾静), Xue-Kui Xi(郗学奎), Wen-Hong Wang(王文洪), and Yong-Chang Lau(刘永昌)
Chin. Phys. B, 2024, 33 (**7**): 077504. DOI: 10.1088/1674-1056/ad34c8

Enhanced anomalous Hall effect in kagome magnet $YbMn_6Sn_6$ with intermediate-valence ytterbium

Longfei Li(李龙飞), Shengwei Chi(迟晟玮), Wenlong Ma(马文龙), Kaizhen Guo(郭凯臻), Gang Xu(徐刚), and Shuang Jia(贾爽)
Chin. Phys. B, 2024, 33 (**5**): 057501. DOI: 10.1088/1674-1056/ad322d

Angular and planar transport properties of antiferromagnetic V_5S_8

Xiao-Kai Wu(吴晓凯), Bin Wang(王彬), De-Tong Wu(吴德桐), Bo-Wen Chen(陈博文), Meng-Juan Mi(弭孟娟), Yi-Lin Wang(王以林), and Bing Shen(沈冰)
Chin. Phys. B, 2024, 33 (**2**): 027503. DOI: 10.1088/1674-1056/ad15f9

Magnetic and electronic properties of bulk and two-dimensional $FeBi_2Te_4$: A first-principles study

Qianqian Wang(王倩倩), Jianzhou Zhao(赵建洲), Weikang Wu(吴维康), Yinning Zhou(周胤宁), Qile Li, Mark T. Edmonds, and Shengyuan A. Yang(杨声远)
Chin. Phys. B, 2023, 32 (**8**): 087506. DOI: 10.1088/1674-1056/acd522

Topological magnetotransport and electrical switching of sputtered antiferromagnetic $Ir_{20}Mn_{80}$

Danrong Xiong(熊丹荣), Yuhao Jiang(蒋宇昊), Daoqian Zhu(朱道乾), Ao Du(杜奥), Zongxia Guo(郭宗夏), Shiyang Lu(卢世阳), Chunxu Wang(王春旭), Qingtao Xia(夏清涛), Dapeng Zhu(朱大鹏), and Weisheng Zhao(赵巍胜)
Chin. Phys. B, 2023, 32 (**5**): 057501. DOI: 10.1088/1674-1056/acb9ec

---

Evolution of anomalous Hall effect in ferromagnetic Weyl semimetal $Nb_xZr_{1-x}Co_2Sn$

Bo-Wen Chen(陈博文)[1,2] and Bing Shen(沈冰)[1,2,†]

[1] *Center for Neutron Science and Technology, Guangdong Provincial Key Laboratory of Magnetoelectric Physics and Devices, School of Physics, Sun Yat-Sen University, Guangzhou* 510275, *China*

[2] *State Key Laboratory of Optoelectronic Materials and Technologies, Sun Yat-Sen University, Guangzhou* 510275, *China*

(Received 10 March 2024; revised manuscript received 22 April 2024; accepted manuscript online 13 May 2024)

Magnetic topological semimetal can host various topological non-trivial states leading to exotic novel transport properties. Here we report the systematic magneto-transport studies on the Heusler alloy $Nb_xZr_{1-x}Co_2Sn$ considered as a ferromagnetic (FM) Weyl semimetal. The cusp anomaly of temperature-dependent resistivity and large isotropic negative magneto-resistivity (MR) emerge around the FM transition consistent with the theoretical half-metallic predictions. The prominent anomalous Hall effect (AHE) has the same behavior with the applied field along various crystal directions. The Nb doping introduces more disorder resulting in the enhancement of the upturn for the temperature-dependent resistivity in low temperatures. With Nb doping, the AHE exhibits systemic evolution with the Fermi level lifted. At the doping level of $x = 0.25$, the AHE mainly originates from the intrinsic contribution related to non-trivial topological Weyl states.

Keywords: anomalous Hall effect, magnetic Weyl semimetal, ferromagnetism

PACS: 75.20.En **DOI:** 10.1088/1674-1056/ad4a3b

1. Introduction

Magnetic topological materials always attract great interest in condensed matter physics.[1] The non-trivial topological state can host various exotic phenomena such as the quantum anomalous Hall effect (QAHE) with chiral edge modes promising great potential for future industrial applications. This effect was first observed in magnetic-doped topological insulator Cr-doped $(Bi,Sb)_2Te_3$ thin film[2] due to the gap opening of the gapless Dirac surface states by introducing the long-range (LR) magnetism. With further studies, its working temperature increases to 1.4 K in an antiferromagnetic (AFM) topological insulators[3,4] $MnBi_2Te_4$ due to the more robust intrinsic LR AFM orders. Another way to realize QAHE is distinguished by the Haldane model[5] which is defined on a honeycomb lattice with real nearest neighbor hopping and next-nearest neighbor hopping. According to this picture, ferromagnetic (FM) kagome topological metals such as FeSn,[6] CoSn,[7] $Co_3Sn_2S_2$[8–12] were widely investigated. Although no quantized Hall conductance was observed, the giant anomalous Hall effect (GAHE) could emerge above liquid nitrogen temperature in these materials. Especially in magnetic kagome $TbMn_6Sn_6$,[13,14] GAHE can persist to 400 K. Besides, a magnetic Weyl semimetal with broken time-reversal symmetry can be interpreted as a stacked heterostructure of such quantum anomalous Hall insulator layers[8] where the coupling between the layers closes the bulk band gap at isolated Weyl nodes. At these Weyl nodes, the Berry curvature is enhanced whereas the carrier density vanishes which may lead to a large or even quantized Hall effect.[8,15] Magnetic Heusler alloy, with the stable structure of a wide variety of elements that can be substituted on any of the three distinct atomic sites within the unit cell, can host several topological properties such as magnetic weyl nodes.[16] The observed GAHE in the half-Heusler compounds GdPtBi,[17] full-Heusler Co_2MnAl,[18] and Co_2MnGa[19] suggests Heusler compounds could be a promising material candidates pool to explore non-trivial topological state and properties.

$ZrCo_2Sn$ is a magnetic Heusler compound and is theoretically predicted as a Weyl semimetal.[16,20] It exhibits half-metallic electron structure and soft ferromagnetism. The Fermi level can be easily engineered and tuned by chemical doping. More importantly, the band structure calculation indicates only a couple of Weyl points close to the Fermi level providing a simple and clear system to study the magnetic Weyl physics.[16] In this paper, we report the systematic transport studies on the $Nb_xZr_{1-x}Co_2Sn$ ($x = 0$–0.5) system. The anomalous Hall effect (AHE) was observed and had the same behavior with the applied field along different directions. Around the FM transition, the negative magneto-resistivity (MR, defined as $MR = (\rho_{xx}(\mu_0 H) - \rho_{xx}(0))/\rho_{xx}(\mu_0 H) \times 100\%$) with a cusp anomaly of temperature-dependent resistivity was observed due to the small Fermi surface and unstable FM state. By doping Nb, the Fermi level of the system was tuned and the anomalous Hall developed from extrinsic region to intrinsic region at the doping level of $x = 0.25$. On the other hand, Nb doping also introduced the disorders leading to the enhancement of upturn of the temperature-dependent resistivity in low-temperature regions. The transport properties of the system exhibited systematic evolution.

†Corresponding author. E-mail: Shenbing@mail.sysu.edu.cn

© 2024 Chinese Physical Society and IOP Publishing Ltd

2. Experimental detail

The single crystals of $Nb_xZr_{1-x}Co_2Sn$ were synthesized by the Sn-flux method. The Zr, Nb, Co, and Sn were mixed stoichiometrically and sealed inside an evacuated quartz tube. The mixture was heated to 1200 °C, slowly cooled to 960 °C, and finally decanted in a centrifuge. The large single crystals were harvested shown in the left inset of Fig. 1(a). The structure and the composition of crystals were checked by x-ray diffraction and wavelength-dispersive spectroscopy (WDS) measurements respectively. The samples were carefully shaped into rectangle bars with the long axis along different crystal directions. Electrical transport measurements were performed in the quantum design physical properties measurement system (QD PPMS Dynacool). The magnetization measurements were performed in the magnetic property measurement system (MPMS).

3. Results and discussion

3.1. The investigation of the anisotropy for $ZrCo_2Sn_2$

The $ZrCo_2Sn$ crystallizes in the *Fm*-3*m* space group as shown in the right inset of Fig. 1(a)[16] and the x-ray diffraction measurements reveal three sets of diffraction peaks of three crystal planes respectively indicating the high-quality crystallization for our samples shown in Fig. 1(a). To investigate the anisotropy of transport properties of $ZrCo_2Sn$, the single crystals were shaped into rectangular devices along various crystal planes. The temperature-dependent resistivity $\rho_{xx}(T)$ of three crystal planes is presented in Fig. 1(b). A cusp anomaly emerges around 170 K related to the FM transition and the negative $d\rho/dT$ is observed in the paramagnetic state breaking down Matthiessen's rule.[21] The similar feature is also observed in other Heusler compounds such as Co_2TiAl etc with the low carrier density due to suppression of the spin fluctuation accompanied with the negative MR.[22] Then the magnetization due to the FM state makes the up and down spin bands split resulting in a half-metallic state. The small Fermi sheets and low carrier density will make the cusp feature (the typical half-metallic feature) become a sharp peak.[23] The observed half-metallic behavior of $Nb_xZr_{1-x}Co_2Sn$ is agreeable with the theoretical calculation. When applying the external field, the MR exhibits a negative response and reaches the maximum with varying temperatures as shown in Fig. 1(c).

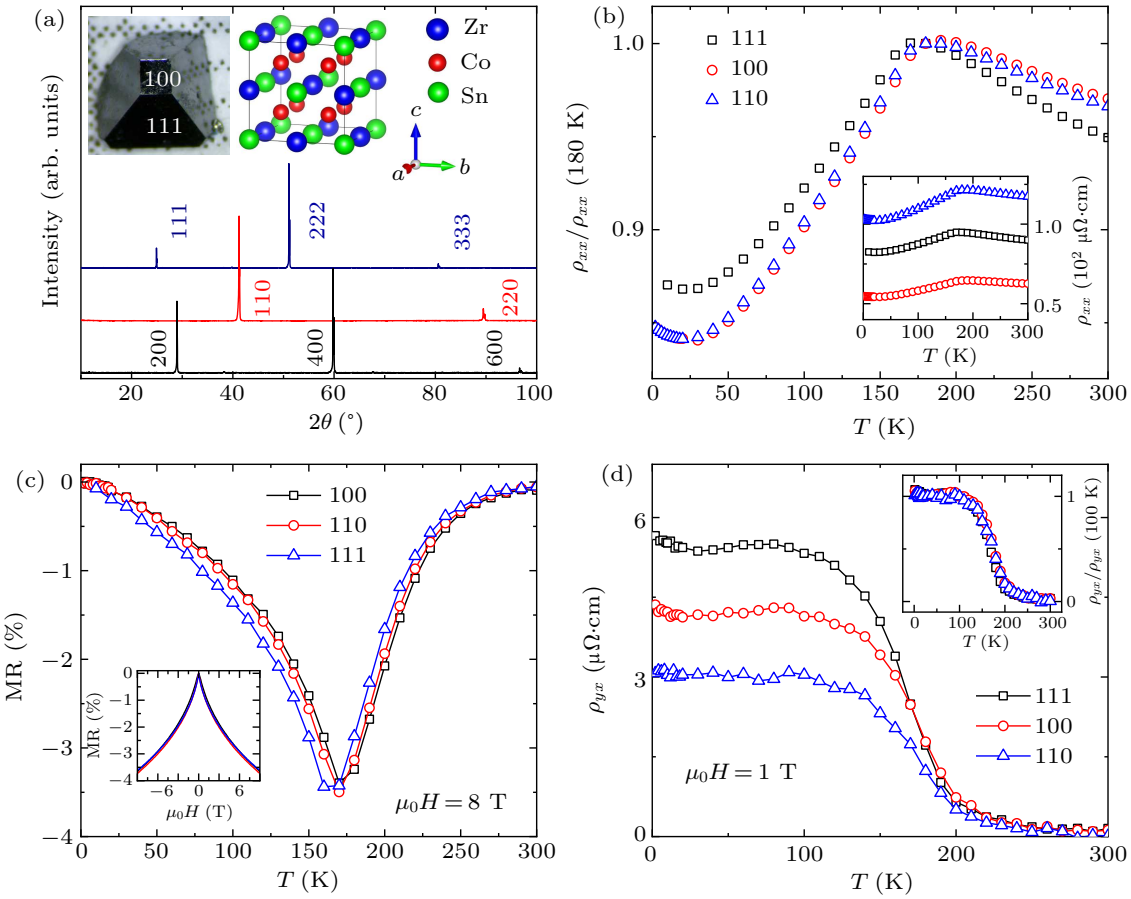


Fig. 1. (a) The x-ray diffraction pattern of the single crystal of $ZrCo_2Sn$. Left inset: the picture of the typical single crystals with the dimensions of 4 mm×3 mm×3 mm. Right inset: the schematic diagram of the $ZrCo_2Sn$ crystal structure. (b) The normalized longitudinal resistivity (ρ_{xx}/ρ_{xx} (180 K)) of $ZrCo_2Sn$ with the current along different crystal planes. The inset: the longitudinal resistivity of $ZrCo_2Sn$ with the current along different crystal planes. (c) The temperature-dependent magneto-resistivity (MR) of $ZrCo_2Sn$ with the current along different crystal planes at 8 T. The inset: the magnetic-field-dependent MR of $ZrCo_2Sn$ with the current along different crystal planes at 170 K. (d) The temperature-dependent Hall resistivity of $ZrCo_2Sn$ with the current along different crystal planes at 1 T. The inset: the normalized Hall resistivity of $ZrCo_2Sn$ with the current along different crystal planes at 1 T.

The temperature-dependent and field-dependent MR of three crystal planes exhibit consistent behavior and even almost the same magnitude, indicating the small anisotropy for $ZrCo_2Sn$. Correspondingly, though the temperature-dependent Hall resistivity of various crystal planes with $\mu_0 H = 1$ T has varied values below the FM transitions, they exhibit same behavior and can overlap by normalizing their value shown in the inset of Fig. 1(d). These identical characters promise $ZrCo_2Sn$ can be changed consistently in different planes during engineering such as doping or pressuring.

3.2. The doping evolution of $ZrCo_2Sn$

According to the theoretical calculations, the Fermi level in $ZrCo_2Sn$ is a little far away from the Weyl points. Thus we introduce Nb to lift the Fermi level to induce non-trivial topological properties. As shown in the left inset of Fig. 2(a), the x-ray diffraction (XRD) peak of [400] plane of $ZrCo_2Sn$ shifts to a higher angle with increasing the doping levels, indicating the a lattice constant shrinking with introducing more Nb (shown in the right inset of Fig. 2(a)). The resistivity increases with the chemical doping accompanied by the emergence of a more and more obvious upturn in low-temperature regions. The evolution of these upturns may result from the Anderson localization due to the disorder originating from the doped impurities.[24] Besides, with the Nb doping, the MR becomes larger in the whole temperature region. At doping level $x = 0.5$ MR exhibits an increase in low-temperature regions consistent with the enhancement of that upturn in $\rho_{xx}(T)$.

It is observed that the cusp anomaly in $\rho_{xx}(T)$ and change in $M(T)$ varies little with Nb doping indicating little suppression of the FM transition. To obtain the accurate FM transition temperature T_c, the Arrott plots of $Nb_xZr_{1-x}Co_2Sn$ ($x = 0$–0.5) are shown in Figs. 3(a)–3(c). According to the theory,[25] the positive value of the intercept acquired by fitting the high-field linear part of the Arrott plots indicates the FM states while the negative value indicates the paramagnetic states. The results reveal the same T_c (195 K±5 K) for $Nb_xZr_{1-x}Co_2Sn$ ($x = 0$–0.5), different from the reported before.[26] Correspondingly, the temperature-dependent magnetization of $Nb_xZr_{1-x}Co_2Sn$ ($x = 0$–0.5) exhibits the same behaviors and close values. These results indicate that the Nb doping does not change the magnetic structure of $Nb_xZr_{1-x}Co_2Sn$. In contrast, the Hall resistivity exhibits prominent evolution. The Hall resistivity and the Hall angle $\Theta = \sigma_{xy}/\sigma_{xx}$ become maximum at $x = 0.25$ prompting us to further investigate the mechanism.

In an FM system, the Hall resistivity can be expressed as

$$\rho_{xy} = \rho_{xy}^{O} + \rho_{xy}^{A} = R_0 \mu_0 H + R_A M, \tag{1}$$

where ρ_{xy}^{O} and ρ_{xy}^{A} are the ordinary Hall resistivity and anomalous Hall resistivity, and R_0 and R_A are ordinary and anomalous Hall coefficient respectively. In high-conductivity FM compounds such as Fe–Ni alloy, the ordinary Hall resistivity is comparable to or even higher than anomalous Hall resistivity.[27] Thus before discussing the AHE, we first estimate the ordinary Hall resistivity of $ZrCo_2Sn$ which is at the order of 0.1 μΩ·cm by using the method in Ref. [28]. The value is much smaller than anomalous Hall resistivity agreeable with the low conductivity of $ZrCo_2Sn$ (1×10^3 S·cm^{-1}–2×10^3 S·cm^{-1}). In the discussion below, we neglect the ordinary Hall contribution and treat anomalous Hall resistivity and anomalous Hall conductivity as $\rho_{xy}^{A} \approx \rho_{xy}$ and $\sigma_{xy}^{A} \approx \sigma_{xy}$.

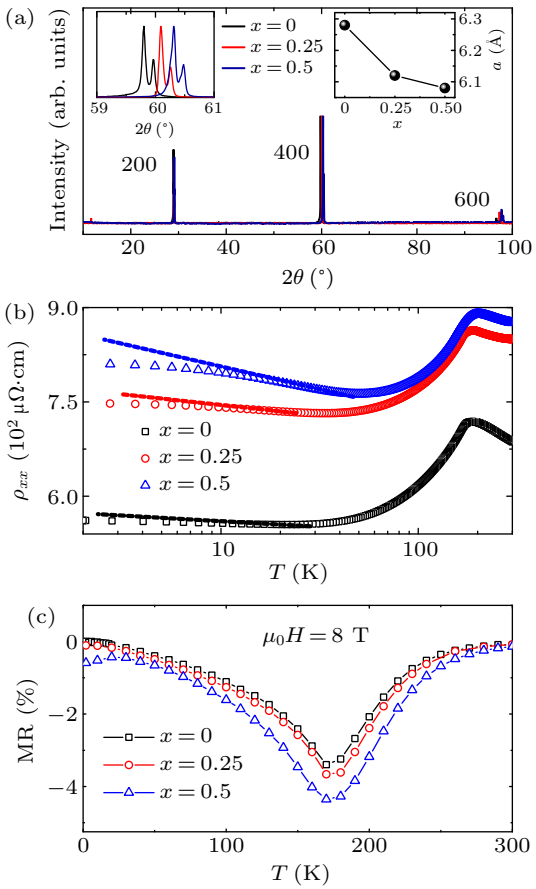


Fig. 2. (a) The x-ray diffraction peaks of [l00] plane of $Nb_xZr_{1-x}Co_2Sn$ ($x = 0$, 0.25, and 0.5) while the 2θ range from 10° to 100°. Left inset: the comparison of x-ray diffraction peaks of [400] plane. Right inset: the lattice constant of $Nb_xZr_{1-x}Co_2Sn$ ($x = 0$, 0.25, and 0.5). (b) Temperature-dependent longitudinal resistivity of $Nb_xZr_{1-x}Co_2Sn$ ($x = 0$, 0.25, and 0.5). (c) The temperature-dependent MR with external field $H = 8$ T of $Nb_xZr_{1-x}Co_2Sn$ ($x = 0$, 0.25, and 0.5).

The AHE contains both extrinsic and intrinsic contribution as: $\sigma_{xy}^{A} = \sigma_{xy}^{A-ex} + \sigma_{xy}^{A-int}$. The extrinsic anomalous Hall term σ_{xy}^{A-ex} due to the impurity such as the side jump and skew scattering strongly depends on the defect and disorder in the system. The intrinsic anomalous Hall term is only related to the Berry curvature of the system as

$$\sigma_{xy}^{A-int} = -\varepsilon_{ijl} \frac{e^2}{\hbar} \Sigma \int \frac{dk}{2\pi} f(k) \Omega(k), \tag{2}$$

where the $\Omega(k)$ is the Berry curvature.[29] In an FM system, Karplus and Luttinger calculated the intrinsic anomalous Hall conductivity $\sigma_{xy}^{\mathrm{A-int}}$ is proportional to the magnetization M as $\sigma_{xy}^{\mathrm{A-int}} \sim M$, which will hold in the case of long-wavelength fluctuations of spin orientation at finite temperature.[30,31] However, one of the extrinsic anomalous contribution, the skew scattering mechanism will deviate this linear dependence of M. Though another extrinsic anomalous contribution, side jump mechanism gives the same relation between σ_{xy} and M as the intrinsic mechanism, its contribution is too small compared to the intrinsic mechanism in the similar system and can be neglected.[32–34] To investigate the mechanism of the AHE for $Nb_xZr_{1-x}Co_2Sn$, the σ_{xy} was calculated by $\sigma_{xy} = \rho_{yx}/(\rho_{xx}^2 + \rho_{xy}^2)$ and plotted versus M by implicitly taking out the dependence on the externally applied magnetic field. As a represent, figure 4(a) shows the plots of σ_{xy} versus M for $Nb_{0.25}Zr_{0.75}Co_2Sn$ at various temperatures below FM transition. The σ_{xy} except for those in low-temperature regions can collapse to one curve exhibiting proportional dependence behavior of M, which is the symbol of the intrinsic contribution. However, in the low-temperature regions below 60 K, the σ_{xy} deviates from the proportional dependence behavior, implying that there exists the extrinsic mechanism, which may be attributed to the impurities induced. When we plot the graph of σ_{xy}/M versus σ_{xx}, the σ_{xy}/M keep a constant independent of σ_{xx} except the low-temperature regions shown in Fig. 4(b). The results indicate the system is dominated by the intrinsic Hall effect except for the low-temperature regions. To further check the evolution of anomalous Hall mechanism, the σ_{xy}/M versus σ_{xx} curves for $Nb_xZr_{1-x}Co_2Sn$ ($x = 0$, 0.25, and 0.5) are presented in Fig. 4(b). With the Nb doping, the σ_{xy}/M first exhibits a weak dependence of σ_{xx} at $x = 0$ and develops into a constant at $x = 0.25$. With further doping Nb, the σ_{xy}/M still exhibits independent behavior of σ_{xx} but has the obvious numerical change at $x = 0.5$, which may be attributed to more impurities induced. In one word, the extrinsic–intrinsic transition for AHE is observed in $Nb_xZr_{1-x}Co_2Sn$ compounds. Besides, σ_{xy}/M in low-temperature regions exhibits a turning and becomes more pronounced with increasing Nb doping. We attribute this anomaly to the disorder and discuss it later.

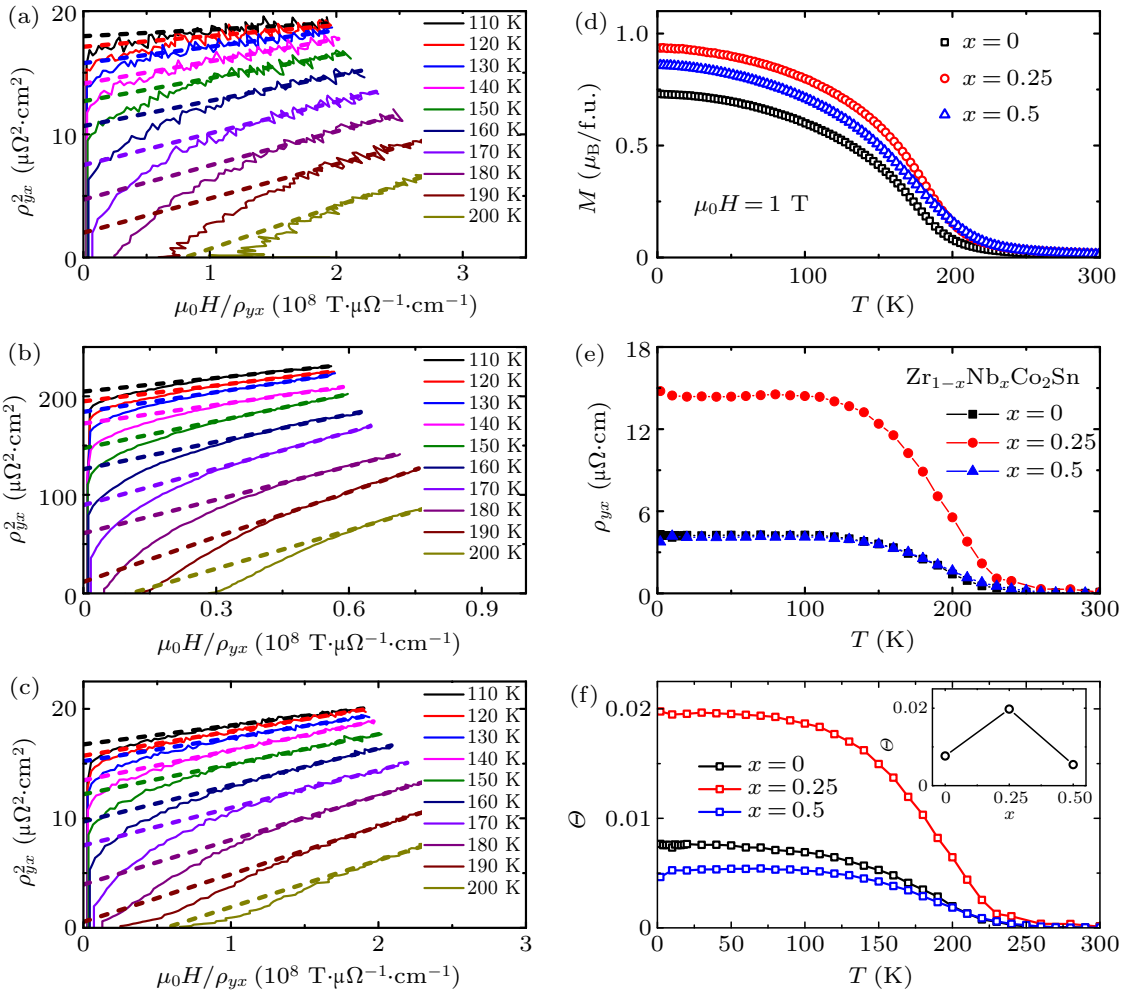


Fig. 3. (a)–(c) The Arrott plots of $Nb_xZr_{1-x}Co_2Sn$ with applied field perpendicular to [100] plane, when the $x = 0$, 0.25, and 0.5, respectively. (d) The temperature-dependent magnetization of $Nb_xZr_{1-x}Co_2Sn$ ($x = 0$, 0.25, and 0.5) with the applied field $\mu_0 H = 1$ T along the c axis. (e) The temperature-dependent spontaneous Hall resistivity of $Nb_xZr_{1-x}Co_2Sn$ ($x = 0$, 0.25, and 0.5). (f) The temperature-dependent Hall angle of $Nb_xZr_{1-x}Co_2Sn$ ($x = 0$, 0.25, and 0.5). The inset: the evolution of the maximum value of Hall angle with different doping levels.

For a clean metal dominated by intrinsic anomalous Hall contribution, the anomalous Hall conductivity is given by the integral of the Berry curvature over all occupied states including the quantized part $\sigma_{xy}^{\mathrm{A-int-q}}$ in Fermi sea and unquantized part $\sigma_{xy}^{\mathrm{A-int-u}}$ from adiabatic motion of quasiparticles on Fermi surface.[15,35] The former is universal to be a topologically quantized value $Ce^2/(2\pi)$ (C is the first Chern number), and the latter is strongly dependent on the Fermi topology (magnetization in ferromagnetic metal). In a magnetic Weyl metal, as long as the Fermi surface is close enough to Weyl points, the part of the intrinsic contribution of the Fermi surface will be absent. In this special case, the universal Fermi surface breaks up into disconnected sheets enclosing each Weyl node and the σ_{xy} will be quantized to $\sigma_{xy}^{\mathrm{quant}} = e^2\kappa/(4\pi^2)$, where κ is the distance between the Weyl nodes.[15] We estimate the quantized $\sigma_{xy}^{\mathrm{quant}}$ to be about 600 S·cm^{-1} for $Nb_xZr_{1-x}Co_2Sn$ system which is larger than 30 S·cm^{-1}. Besides the Hall angle Θ of $Nb_{0.25}Zr_{0.75}Co_2Sn$ in intrinsic anomalous Hall region is 0.020, which is smaller than the value of intrinsic contribution in GdPtBi (Θ to 0.1) due to the spin chirality.[36] This results implies that the Fermi levels may still be not close enough to the Weyl points and the impurities induced by the Nb doping may have passive impact on the intrinsic anomalous contribution.

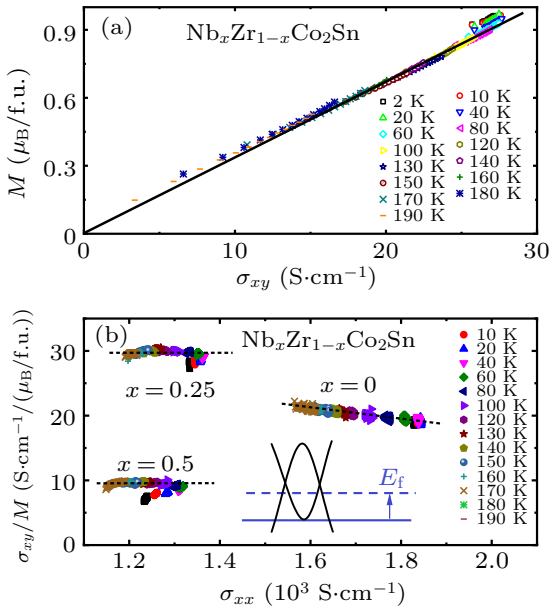


Fig. 4. (a) The M versus σ_{xx} at different temperatures of $Nb_xZr_{1-x}Co_2Sn$ ($x = 0.25$). (b) The σ_{xy}/M versus σ_{xx} for $Nb_xZr_{1-x}Co_2Sn$ ($x = 0$, 0.25, and 0.5). The inset: The schematic diagram of the Fermi level's shift with doping.

Doping Nb into $ZnCo_2Sn$ affects the system in two ways. (i) Changing the scattering of the system: With the Nb doping, the scattering changes due to introducing more disorder. (ii) Changing the Fermi energy instead of the band structure: According to theoretical calculations, by doping Nb, the Fermi energy can be lifted to approach the Weyl nodes. For the former, the system is sensitive to the Nb doping which can be observed in the change of longitudinal and resistivity especially for their upturn behavior in low-temperature regions. The change of Born scattering amplitude $\hbar/\tau$ of the system due to disorder introduced by Nb doping results in the extrinsic-to-intrinsic crossover.[37] For the latter, the unqualified σ_{xy} indicates besides the Weyl nodes the quasiparticle around the Fermi surface (trivial state) still contributes the intrinsic AHE where the Fermi level is not close to the Weyl points enough.

4. Conclusion

In conclusion, we have systemically studied the magneto-transport of Heusler half-metal $Nb_xZr_{1-x}Co_2Sn$, a proposed candidate of FM Weyl semimetal. The isotropic negative MR was observed with the maximum around FM transition with a cusp feature indicating the half-metallic behavior of $Nb_xZr_{1-x}Co_2Sn$. The obvious AHE was experimentally observed and had the same behavior with the applied field along different crystal directions. With the Nb doping, the AHE exhibited systemic evolution behavior. At the doping level of $x = 0.25$, the σ_{xy} reached the maximum and originated from the intrinsic anomalous Hall mechanism.

Acknowledgements

Project supported by the National Key Research and Development Program of China (Grant Nos. 2023YFF0718400 and 2023YFA1406500), the National Natural Science Foundation of China (Grant Nos. U2130101 and 92165204), the Natural Science Foundation of Guangdong Province, China (Grant No. 2022A1515010035), the Open Project of Guangdong Provincial Key Laboratory of Magnetoelectric Physics and Devices (Grant No. 2022B1212010008), and the Open Project of Key Laboratory of Optoelectronic Materials and Technologies (Grant No. OEMT-2023-ZTS-01).

References

[1] Bernevig B A, Felser C and Beidenkopf H 2022 *Nature* **603** 41
[2] Chang C Z, Zhang J, Feng X, Shen J, Zhang Z, Guo M, Li K, Ou Y, Wei P, Wang L L, Ji Z Q, Feng Y, Ji S, Chen X, Jia J, Dai X, Fang Z, Zhang S C, He K, Wang Y, Lu L, Ma X C and Xue Q K 2013 *Science* **340** 167
[3] Otrokov M M, Klimovskikh I I, Bentmann H, *et al.* 2019 *Nature* **576** 416
[4] Deng Y, Yu Y, Shi M Z, Guo Z, Xu Z, Wang J, Chen X H and Zhang Y 2020 *Science* **367** 895
[5] Haldane F D M 1988 *Phys. Rev. Lett.* **61** 2015
[6] Kang M, Ye L, Fang S, You J S, Levitan A, Han M, Facio J I, Jozwiak C, Bostwick A, Rotenberg E, Chan M K, McDonald R D, Graf D, Kaznatcheev K, Vescovo E, Bell D C, Kaxiras E, van den Brink J, Richter M, Prasad Ghimire M, Checkelsky J G and Comin R 2020 *Nat. Mater.* **19** 163
[7] Kang M, Fang S, Ye L, Po H C, Denlinger J, Jozwiak C, Bostwick A, Rotenberg E, Kaxiras E, Checkelsky J G and Comin R 2020 *Nat. Commun.* **11** 4004

[8] Liu E, Sun Y, Kumar N, Muechler L, Sun A, Jiao L, Yang S Y, Liu D, Liang A, Xu Q, Kroder J, Süß V, Borrmann H, Shekhar C, Wang Z, Xi C, Wang W, Schnelle W, Wirth S, Chen Y, Goennenwein S T B and Felser C 2018 *Nat. Phys.* **14** 1125

[9] Liu D F, Liang A J, Liu E K, Xu Q N, Li Y W, Chen C, Pei D, Shi W J, Mo S K, Dudin P, Kim T, Cacho C, Li G, Sun Y, Yang L X, Liu Z K, Parkin S S P, Felser C and Chen Y L 2019 *Science* **365** 1282

[10] Liu E, Sun Y, Kumar N, Muechler L, Sun A, Jiao L, Yang S Y, Liu D, Liang A, Xu Q, Kroder J, Süß V, Borrmann H, Shekhar C, Wang Z, Xi C, Wang W, Schnelle W, Wirth S, Chen Y, Goennenwein S T B and Felser C 2018 *Nat. Phys.* **14** 1125

[11] Wang Q, Xu Y, Lou R, Liu Z, Li M, Huang Y, Shen D, Weng H, Wang S and Lei H 2018 *Nat. Commun.* **9** 3681

[12] Yang H, You W, Wang J, Huang J, Xi C, Xu X, Cao C, Tian M, Xu Z A, Dai J and Li Y 2020 *Phys. Rev. Mater.* **4** 024202

[13] Gao L, Shen S, Wang Q, Shi W, Zhao Y, Li C, Cao W, Pei C, Ge J Y, Li G, Li J, Chen Y, Yan S and Qi Y 2021 *Appl. Phys. Lett.* **119** 092405

[14] Yin J X, Ma W, Cochran T A, Xu X, Zhang S S, Tien H J, Shumiya N, Cheng G, Jiang K, Lian B, Song Z, Chang G, Belopolski I, Multer D, Litskevich M, Cheng Z J, Yang X P, Swidler B, Zhou H, Lin H, Neupert T, Wang Z, Yao N, Chang T R, Jia S and Zahid Hasan M 2020 *Nature* **583** 533

[15] Burkov A A 2014 *Phys. Rev. Lett.* **113** 187202

[16] Wang Z, Vergniory M G, Kushwaha S, Hirschberger M, Chulkov E V, Ernst A, Ong N P, Cava R J and Bernevig B A 2016 *Phys. Rev. Lett.* **117** 236401

[17] Suzuki T, Chisnell R, Devarakonda A, Liu Y T, Feng W, Xiao D, Lynn J W and Checkelsky J G 2016 *Nat. Phys.* **12** 1119

[18] Li P, Koo J, Ning W, Li J, Miao L, Min L, Zhu Y, Wang Y, Alem N, Liu C X, Mao Z and Yan B 2020 *Nat. Commun.* **11** 3476

[19] Sakai A, Mizuta Y P, Nugroho A A, Sihombing R, Koretsune T, Suzuki M T, Takemori N, Ishii R, Nishio-Hamane D, Arita R, Goswami P and Nakatsuji S 2018 *Nat. Phys.* **14** 1119

[20] Sklyadneva I, Heid R, Echenique P M and Chulkov E V 2021 *Phys. Rev. B* **103** 024303

[21] Matthiessen A and Vogt C 1864 *Ann. Phys.* **198** 19

[22] Barth J, Fecher G H, Balke B, Ouardi S, Graf T, Felser C, Shkabko A, Weidenkaff A, Klaer P, Elmers H J, Yoshikawa H, Ueda S and Kobayashi K 2010 *Phys. Rev. B* **81** 064404

[23] Kataoka M 2001 *Phys. Rev. B* **63** 134435

[24] Kamble R B, Tanty N, Patra A and Prasad V 2016 *Appl. Phys. Lett.* **109** 083102

[25] Arrott A 1957 *Phys. Rev.* **108** 1394

[26] Yang M, Gu G, Yi C, Yan D, Li Y and Shi Y 2019 *J. Phys.: Condens. Matter* **31** 275702

[27] Friedemann S, Brando M, Duncan W J, Neubauer A, Pfleiderer C and Grosche F M 2013 *Phys. Rev. B* **87** 024410

[28] Checkelsky J G, Lee M, Morosan E, Cava R J and Ong N P 2008 *Phys. Rev. B* **77** 014433

[29] Nagaosa N, Sinova J, Onoda S, MacDonald A H and Ong N P 2010 *Rev. Mod. Phys.* **82** 1539

[30] Zeng C, Yao Y, Niu Q and Weitering H H 2006 *Phys. Rev. Lett.* **96** 037204

[31] Huang Y Q, Zheng P Y, Liu R, Xu X T, Wu Z Y, Dong C, Wang J F, Yin Z P and Jia S 2023 *Chin. Phys. B* **32** 107502

[32] Shukla G K, Sau J, Shahi N, Singh A K, Kumar M and Singh S 2021 *Phys. Rev. B* **104** 195108

[33] Liu Y, Tan H, Hu Z, Yan B and Petrovic C 2021 *Phys. Rev. B* **103** 045106

[34] Wang Q, Sun S, Zhang X, Pang F and Lei H 2016 *Phys. Rev. B* **94** 075135

[35] Haldane F D M 2004 *Phys. Rev. Lett.* **93** 206602

[36] Nayak A K, Fischer J E, Sun Y, Yan B, Karel J, Komarek A C, Shekhar C, Kumar N, Schnelle W, Kbler J, Felser C and Parkin S S P 2016 *Sci. Adv.* **2** e1501870

[37] Onoda S, Sugimoto N and Nagaosa N 2006 *Phys. Rev. Lett.* **97** 126602